

Synthesis, spectral and thermal characterization, and biomolecular docking of Pd(II) and Pt(II) complexes with (E)-3-(4-(dimethylamino)phenyl)-1-(pyridin-2-yl)prop-2-en-1-one.

Mohamed Gaber* ¹, Hoda A. El-Ghamry ^{1, 2}, Mohammed A. Mansour³

¹Chemistry Department, Faculty of Science, Tanta University, Tanta, Egypt

²Department of Chemistry, Faculty of Applied Science, Umm Al-Qura University, Makkah, Kingdom of Saudi Arabia

³Biochemistry Division, Department of Chemistry, Faculty of Science, Tanta University, Tanta 31527, Egypt

Keywords: Chalcones; Pt(II),Pd(II) complexes; Molecular Docking, Anticancer

*Address correspondence to:

Mohammed Gaber, PhD; Department of Chemistry, Faculty of Science, Tanta University, Tanta 31527, Egypt; E-mail: mabuelazm@science.tanta.edu.eg

Abstract

Pd (II) and Pt(II) complexes of (E)-3-(4-(dimethylamino)phenyl)-1-(pyridin-2-yl) prop-2-en-1-one (L) and its Pd (II) and Pt(II) formulated as $[\text{Pt}(\text{L}_1)_2] \text{Cl}_2 \cdot 2\text{H}_2\text{O}$, $[\text{Pd}(\text{L}_1)_2] \text{Cl}_2 \cdot 0.5\text{H}_2\text{O}$, $[\text{Pd}(\text{L}_1)_2] (\text{AcO})_2 \text{CH}_3\text{OH}$ have been synthesized. Elemental analyses, molar conductance, thermal technique, molecular modeling, IR and electronic spectral measurements were used to verify the structures of the complexes. The titled ligand behaves as neutral bidentate ligand coordination via pyridine nitrogen and carbonyl oxygen. These complexes are with square planar geometry. The kinetic and thermodynamic parameters of the decomposition steps were evaluated. The in-vitro antimicrobial and antitumor activities of the investigated compounds were screened against different microorganisms and the human hepatocellular carcinoma cells, HEPG2, respectively. The data showed that the metal complexes have more antimicrobial and antitumor activities than the ligand itself. Molecular docking studies were performed by DockingServer and SwissDock using X-ray crystallographic structures of the proteins (3t88, 4m01, 4ynt, 1zap & 121P) from Protein Data Bank (PDB). The ligand and possibly its complexes showed favorable binding with the receptors of the microorganisms (3t88, 4m01, 4ynt, 1zap) and H-ras oncoprotein. Hence, our results present the synthesized complexes as potential antimicrobial and anticancer drug candidates.

1. Introduction

Platinum (II) complexes such as cis-platin, carboplatin, oxaliplatin have been extensively used as anticancer drugs. The most striking example is cisplatin, however it has encountered many side effects. Due to the accompanied severe side effects, drug resistance and the limited spectrum of tumors, great efforts have been made to synthesize several transition metal complexes to replace the conventional chemotherapy with low doses and high efficacy. Special attention in this regard has been given to palladium (II) complexes. Due to the structural and thermodynamic analogy between Pt(II) and Pd(II) complexes, a number of palladium (II) complexes with their potential antitumor properties have been reported [1-26]. Recent studies on the design of less toxic and more selective metal-based antitumor drugs are directed to the biologically interesting ligands. The nature of the ligands and the metal coordination pattern play an important role for the antitumor properties of the complexes. With this regard, chalcone derivatives are very interesting ligand candidates due to their broad spectrum of biological activities and potential applications such as anti-bacterial, anti-inflammatory, antitumoral, antimalarial, as well as antioxidant properties [27-32]. Hence, in the current study, the transition metal complexes of chalcones and related compounds have been studied due to their interesting behavior in catalytic and biological applications [33-43].

We described here the synthesis of Pd(II) and Pt(II) complexes of the titled chalcone compound (**Fig. 1**). The structures of the metal complexes were proposed on the basis of elemental analyses, spectral and molecular modeling as well as the thermal measurements (**Fig. 2**). The antibacterial activities of the synthesized compounds were screened in vitro against gram-positive bacteria and gram-negative bacteria as well as antifungal activity against the two fungal strains *Aspergillus flavus* and *Candida albicans*. The antitumor activity was studied against the human hepatocarcinoma cells HEPG2. Molecular docking analysis was performed

to test the ligand for its inhibitory activity on the receptor of *Escherichia coli* (3t88), *Staphylococcus aureus* adhesion protein (4m01), *Aspergillus flavus* FAD glucose dehydrogenase (4ynt) and secreted aspartic protease from *Candida albicans* (1zap). Besides, to elucidate the proposed mechanism of the antitumor activity of the ligand, molecular docking was performed against the oncogenic protein H-ras (PDB: 121p). Different parameters like FullFitness, Gibbs free energy (ΔG), free energy of binding, inhibition constant (K_i), total energy of Van der Waals (vdW) force + hydrogen bond (Hbond) + desolv energy (EVHD), electrostatic energy, total intermolecular energy, frequency of binding, ligand bond, non-ligand bond, hydrogen bond, and its length were studied. A complete interaction profile (hydrogen bonds, polar, hydrophobic, pi-pi, cation-pi and others), and hydrogen bonding interactions (HB plot) were also studied.

2. Experimental

2.1. Chemicals

All materials used in the present work were of analytical grade and used as received. K_2PtCl_4 , K_2PdCl_4 and $Pd(AcO)_2$, metal salts were used for the preparation of the complexes C1, C2 and C3, respectively. Chalcone compound (Fig. 1) was synthesized and characterized according to the method reported previously [34,40].

2.2. Synthesis of metal complexes.

A solution of the appropriate metal ion (0.01 mol) in EtOH (10 ml) was mixed with a solution of the chalcone derivative (0.01 mol) in the same solvent (30 ml) in the molar ratio 1:2 (M:L) and the resulting mixture was then stirred under reflux for 3 h upon which the complexes were precipitated during reflux. The precipitated complexes were then filtered off, washed several times with ethanol, dried and kept in desiccators over silica gel. The structures of the complexes are shown in Fig. 2.

Complex 1: C1 [Pt(L₁)₂] Cl₂ ·2H₂O: Anal. Calcd. For (C₃₂H₃₆Cl₂ PtN₄O₄) (FW: 806.64): C, 47.65; H, 4.50 ; N, 6.95 ; found: C, 47.89; H, 4.25 ; N, 6.85 %.

Complex 2: C2 [Pd (L₁)₂] Cl₂ 0.5H₂O: Anal. Calcd. For (C₃₂H₃₃Cl₂ PtN₄O_{2.5}) (FW: 690.96): C, 55.62; H, 4.81; N, 8.11; found: C, 55.33; H, 4.70; N, 7.98 %.

Complex 3: C3 [Pd (L₁)₂] (AcO)₂ CH₃OH: Anal. Calcd. For (C₃₇H₄₂N₄O₇ Pd) (FW: 761.17): C, 58.38; H, 5.56; N, 7.36; found: C, 58.21; H, 5.45; N, 7.28 %.

2.3. Measurements

Microanalyses of C, H and N were performed using Heraeus CHN elemental analyzer. The electron impact mass spectra were recorded using a Finnigan MAT8222 spectrometer at 70 eV. The IR spectra were measured, as KBr discs, on a Perkin Elmer 1430 spectrophotometer in the 4000–200 cm⁻¹ range. Shimadzu 240 UV–vis spectrometer was used for the electronic spectral studies. Computerized Shimadzu TG-50 thermal analyzer was applied for the thermal analysis (TGA) up to 800 °C at a heating rate 10 °C/min in an atmosphere of N₂. Molar conductivities in DMF (10⁻³ M) at room temperature (25 °C) were measured by the aid of conductance bridge of the type 523 conductivity bridge.

Molecular docking using DockingServer

Docking calculations were carried out using Docking Server [44]. Originals semiempirical charges calculated by MOPAC2009 (J. P. Stewart, Computer code MOPAC2009, Stewart Computational Chemistry, 2009) were added to the ligand atoms. Non-polar hydrogen atoms were merged, and rotatable bonds were defined. Docking calculations were carried out on receptor of Escherichia coli (3t88), Staphylococcus aureus adhesion protein (4m01), Aspergillus flavus FAD glucose dehydrogenase (4ynt), secreted aspartic protease from

Candida albicans (1zap) and the oncogenic protein H-ras (121p) models. Essential hydrogen atoms, Kollman united atom type charges, and solvation parameters were added with the aid of AutoDock tools [45].

Affinity (grid) maps of 20×20×20 Å grid points and 0.375 Å spacing were generated using the Autogrid program [45]. AutoDock parameter set- and distance-dependent dielectric functions were used in the calculation of the van der Waals and the electrostatic terms, respectively. Docking simulations were performed using the Lamarckian genetic algorithm (LGA) and the Solis & Wets local search method [46].

Molecular docking using SwissDock

Molecular Docking calculations were performed also using SwissDock service based on the docking software EADock DSS [47]. This web-based service was selected because it has user friendly interface with the facility to input desired protein and ligand structures directly from databases, modify docking parameters, and visualize most favorable clusters online. Moreover, results can be viewed in UCSF Chimera package. A grid (Box size: 40×40×40) and box center: 0.38×−2.98×20.51 for x,y, and z, respectively) was designed in which many binding modes were generated for the most favorable bindings. Simultaneously, their CHARMM energies are estimated on the grid [48] Binding modes were scored using their FullFitness and clustered. Clusters were then ranked according to the average FullFitness of their elements [49]. Results of the SwissDock were visualized by UCSF Chimera package [50].

2.4. Biological activity

Disc diffusion method [51] was employed to evaluate the antimicrobial activity, Freshly prepared spore suspension of different microorganisms (0.5 ml of 10⁶ cells/ml) was mixed with 9.5 ml of melting sterile Sabouraud's dextrose medium (for fungi) or nutrient agar medium (for bacteria) at 45 °C, poured on sterile Petri dishes, and left to solidify at

25°C. Regular cellulose filter paper discs (6 mm diameter) were prepared under aseptic conditions. Each disc was saturated with 20 mg of each tested suspended material. Three replicas were made for each test, and all plates were incubated at 27 °C for 48 hours for fungi, and at 32 °C for 24 hours for bacteria. Then the average diameters (mm) of inhibition zones were recorded.

MIC determination

Half-fold serial dilutions were made for selected complexes in order to prepare concentrations of 6.25, 12.5, 25, 50 and 100 mg/ml in distilled water. Zero concentration was considered as a negative control. A previously prepared pure spore suspension of each test microorganism (0.5 ml of about 10^6 cells/ml) was added to 9.5 ml of each concentration in sterile test tubes, incubated at 27 °C for 3 days for fungi, and at 32 °C for 24 hours for bacteria. The optical density of growth was measured by spectrophotometer (Optima SP-300, Japan) at 620 nm for each incubated mixture, results were represented graphically, and MIC was recorded for each tested material [52].

2.5. Measurement of Potential cytotoxicity by SRB assay.

HEPG2 Human cancer cell line was used for in vitro screening experiments. This cell line was obtained frozen in liquid nitrogen (-180 °C) from the American Type Culture Collection. The tumor cell line was maintained in the National Cancer Institute, Cairo, Egypt, by serial sub-culturing. Potential cytotoxicity of the compounds was tested using Skehan et. al. method [53]. Cell was plated in 96-multiwell plate (104 cells/well) for 24 hrs before treatment with the compound to allow attachment of cell to the wall of the plate. Different concentrations of the compounds under study (0, 5, 12.5, 25 and 50 µg/ml) were added to the cell monolayer triplicate wells prepared for each individual dose. The monolayer cell was incubated with the compounds for 48 hrs at 37 °C and in atmosphere of 5% CO₂. After 48 hrs, Cell was fixed, washed and stained

with the protein-binding dye Sulfo-Rhodamine-B (SRB) [54]. Excess stain was washed with acetic acid and attached stain was recovered with Tris-EDTA buffer. Color intensity was measured in an ELISA reader. The relation between surviving fraction and drug concentration is plotted to get the survival curve of each tumor cell line after the specified compound. Potential cytotoxicity of the compounds was measured in (Pharmacology Unit, Cancer Biology Department, National Cancer Institute, Cairo University). Doxorubicin was used as standard cytotoxins.

2.6. DPPH radical scavenging.

1 µg of the studied samples and ascorbic acid (reference compound) were dissolved in DMSO (1 ml). 250 µl of each solution was added to 1 ml DPPH/DMSO solution (6 mg/50 ml) and the total volume was adjusted to 3 ml with DMSO. The mixture was incubated for 30 min at room temperature. Absorbance was measured at 517 nm. The blank sample containing the same amount of DMSO and DPPH solution was prepared and measured as well. The experiment was carried out in triplicate. The scavenging potential was compared with a solvent control (0% radical scavenging) and ascorbic acid. Radical scavenging activity was calculated from the following formula:

$$\% \text{ Reduction of absorbance} = [(X - Y)/X] \times 100$$

Where: X and Y are the absorbance of blank sample and tested sample, respectively.

2.7. Molecular modeling and quantum chemical parameters.

Several attempts to grow appropriate crystals for X-ray crystallography were unsuccessful. Using theoretical parameters help to characterize the molecular structure of the investigated complexes. Due to this problem, the geometries of the complexes were optimized by hyper chem. 8.03

Molecular Modeling and Analysis Program[55] using the molecular mechanics calculations (PM3).

3. Results and Discussion

3.1. Characterization of the solid complexes

3.1.1. Analytical data

Structure elucidation of Pd(II) and Pt(II) complexes was accomplished by elemental analyses, IR, electronic spectra and conductance measurements as well as thermal analysis (TGA). The analytical data are in a good agreement with the proposed structure. The solid complexes are stable in air and easily soluble in DMF and DMSO. For complexes C1 and C2, The presence of Cl⁻ ions outside the coordination sphere was confirmed by the chemical reaction with AgNO₃ where the white precipitate of AgCl was observed. The melting points of the complexes are higher than that of the ligand revealing that the complexes are much more stable than the ligand. For complex C3, The addition of FeCl₃ solution to complex solution gave the red brown coloration confirming that the acetate ions are present outside the coordination sphere.

The molar conductance values of Pd(II) and Pt(II) complexes in 10⁻³ M DMF as solvent are 83.9, 81.2 and 77.5 ohm⁻¹ cm² mol⁻¹ for complexes C1, C2 and C3, respectively. These values revealed that all the complexes are electrolytes in nature i.e. the counter ions present outside the coordination sphere of the metal complexes [56]. These data indicate the formation of 1:2 (M:L) complexes of the formula [ML₂]X₂.nH₂O, where M represents Pd(II) and Pt(II); L represents the ligand; X=Cl for complexes C1 and C2; X=AcO for complex C3; n= 2, 0.5 and 1 for complexes C1, C2 and C3, respectively.

3.1.2. Spectral studies

A comparison of the IR spectrum of the free chalcone with that of the metal complexes was carried out to investigate the mode of bonding of the

ligand to metal centers (**Table 1**). In the IR spectra of the complexes, the band characteristic for C=O bond is shifted to lower frequency compared with that of the free ligand indicating the coordination of the carbonyl oxygen to the metal ion. This shift is mainly due to weakening of the double bond between carbon and oxygen. The stretching vibration of the C=N bond of the pyridine ring is shifted to lower wavenumbers in the spectra of the complexes. This shift indicated the coordination of the pyridine nitrogen atom to the metal ion. The participation of the carbonyl oxygen and pyridine nitrogen was also confirmed by the appearance of a new bands in the spectra of the complexes within the ranges 597-630 and 555-560 cm^{-1} corresponding to M ←N and M←O bond, respectively. These results indicated that the chalcone ligand behaved as neutral bidentate ligand coordinating via the nitrogen and oxygen atoms of pyridine ring and carbonyl group, respectively.

The electronic spectra of the complexes were recorded as Nujol mull. The band at 358 and 360 nm in the spectra of Pt(II) complex C1 and Pd(II) complex C2, respectively, are assignable to a combination of $1A_{1g} \rightarrow 1E_g$ and MLCT indicating square planar geometry around the metal center [57], as expected. The broad bands observed at 580 and 570 nm are assigned to ($1A_{1g} \rightarrow 1B_{1g}$) transition for complexes C2 and C3, respectively, confirming the expected square planar geometry [58].

The constitution and purity of the prepared complexes are confirmed using the electron impact mass spectrometry (EI). **Fig. S1** represents the mass spectrum of C1, as a representative example. The EI mass spectra of the metal complexes showed the molecular ion peaks at $m/z = 804$, 691 and 761 for complexes C1, C2 and C3, respectively, which are highly comparable with the molecular mass of the respective metal complexes. The fragmentation pathways of the metal complexes are shown in **Schemes S1-S3**.

3.1.3. Thermal analysis and kinetic parameters

The thermal behavior of the metal complexes was studied using TG technique (**Fig. S2**). The stages of decomposition, temperature ranges, weight loss percentages as well as decomposition products are given in **Table 2**. The metal percentages of the complexes were calculated from the residual metal oxides formed as a final product. The thermal decomposition of complexes (**1-3**) comprises three steps.

For Pt(II) complex C1 the first step of decomposition occurred within the temperature range 30-87 °C with mass loss 3.98 % (cal. 4.46 %), corresponding to the volatilization of hydrated water molecule. The second step appeared at 87-316 °C with mass loss 13.93 % (cal. 14.3 %) due to elimination of Cl + N(CH₃)₂ moiety. The third step(appearing at 316-428 °C with mass loss 43.11 % (cal. 43.62 %), represented the degradation of the organic ligand with formation of PtO + 8C as final products. For complex C2, the first step appeared at 30-85 °C with mass loss 1.48% (cal. 1.3%) correspond to elimination of molecule of hydration water. The second step appeared at 163- 252 °C with mass loss 14.85 % (cal. 14.47 %) which can be assigned to the loss of Cl⁻ anions and 2CH₃. The third step appearing at 252-447 °C with mass loss 54.74 % (cal. 54.49 %), corresponded to the decomposition of the organic ligand with the formation of PdO + 7C as a final product. The thermal decomposition of Pd(II) complex **C3** showed first step at 25-76 °C with mass loss 3.84 % (cal. 4.2 %) which corresponded to elimination of lattice methanol molecule. The second step at 76-283 °C with mass loss 31.72 % (cal. 31.34%) and assigned to elimination of N(CH₃)₂, C₆H₅ and two acetate anions. The third step appearing at 283-423 °C with mass loss 36.66% (cal 37.42 %) correspond to further decomposition of the organic ligand with formation of PdO + 7C.

The kinetic parameters of decomposition process of the complexes namely, activation energy (E), the order (n) and pre-exponential factor (A), as well as the thermodynamic parameters (enthalpy ΔH, entropy ΔS and free energy of the decomposition ΔG) were evaluated graphically by using

Coats–Redfern [59]. The linearization curves (Fig. 3) of the Coats–Redfern method are shown in supplementary data. The calculated values of n , E , A , ΔS , ΔH and ΔG for the decomposition steps are given in Table 3. According to the data obtained, the following remarks can be pointed out:

The high values of (ΔE) reflected the high stability of the investigated complexes due to their covalent character [60]. The positive sign of ΔG for the investigated metal complexes revealed that all the decomposition steps are non-spontaneous processes. The negative values of ΔS indicated a more ordered activated complex than reactant and/or the reaction was slow [61]. The positive values of ΔH^* means the endothermic decomposition processes.

3.1.4. Molecular modeling

Several attempts to grow appropriate crystals for X-ray crystallography were unsuccessful. The computational strategy in this manuscript is to determine the geometry of Pd(II) complex. Thus, molecular modeling calculations were considered.

Geometrical optimization

The optimized geometries and numbering of atoms of the ligand and its Pd(II) complex are shown in Fig.4. The optimized lengths of the bond and angles of the bond (supplementary materials) are listed are listed in Table S1 & S2.

The elongation of the bond lengths for the C=O and C-N of the pyridine moiety indicated that these bonds become weaker due to the formation of Pd-O and Pd-N bonds. M-O bond length is shorter than M-N bond length showing that the bond length obeyed the order M-N > M-O. The Pd-N_{py} bond length (1.9859, 1.9711) is in agreement with the reported values [62] observed for Pd(II) complexes. C8-C9, C9-C10, C28-C29 and C29-C30 bond lengths become shorter confirming the participation of O and N atoms in complex formation. The bond length of CH=CH (C7-C8, C27-

C28) decreased in complex formation. The bond angle in complex lie in the range for square planar geometry. The C10- C9-O19 and C30-C29-O39 angles change from 117.95 ° to 121.36 and 120.26 ° ,respectively, due to the formation of O19- Pd20- N15 and O39- Pd20- N35 ring.

Molecular parameters

Quantum chemical parameters of compounds such as the energy of the highest occupied molecular orbital, E_{HOMO} , energy of the lowest unoccupied molecular orbital, E_{LUMO} , energy gap (ΔE) electronegativity (χ), chemical potentials (P_i), dipole moment (μ), hardness (η), softness (σ), additional electronic charge (ΔN_{max}) have been calculated according to the equations in the literature.[63-65]. The data are listed in **Table 4**. **Fig. 5** shows the HOMO and LUMO molecular orbitals of the ligand and its Pd(II) complex. The energy components are listed in **Table 5**. The energies of the HOMO and LUMO are negative which indicate that the compounds under investigation are stable [66]. The calculated energy of E_{LUMO} level shows that ligand (-3.334) has lower energy of E_{LUMO} than the complex (-1.105). The calculated HOMO-LUMO energy gap **or energy seperation** (ΔE) of the ligand (5.666) is lower than that of the complex.(6.186). The calculated HOMO-LUMO energy gap **or energy seperation** (ΔE) is related to polarizability, softness and charge migration during the enzyme-drug interaction. As the value of (ΔE) decrease (Pd 6.186 \rightarrow Lig. 5.666), softness (Pd 0.3223 \rightarrow Lig. 0.35), anticancer (IC50, Pd 3.98 \rightarrow Lig. 6.53), and antibacterial activity_ (Pd 15 \rightarrow Lig. 11), of the compound increased.

The binding energy of complex (-7.748 x 10³ k cal/ mol) is higher than that of the ligand (-3.684 x 10³ k cal / mol) indicating the higher stability of the formed metal complex. The negative binding energy indicated that the complexation process is energetically favourable. The negative value of enthalpy change (ΔH) indicated that the interaction between the ligand and Pd(II) ion is exothermic. The dipole moment is important physical quantity which reflects the ability of interaction of the molecules with the

surrounding environment. The dipole moment of complex (5.788) is higher than that of the ligand (3.421). Thus, the Pd(II) complex is the promising structure for antitumor agent. The positive electrophilicity index value indicate the molecule capable of accepting electrons from the environment.

Docking

The parameters of free energy of binding, inhibition constant (K_i), total estimated energy of vdW+Hbond+desolv(EVHD), electrostatic energy, total intermolecular energy, frequency of binding, and interact surface area were evaluated to estimate the favorable binding of the ligand to the protein. Table 6 shows the complete profile of these parameters of the ligand for its interaction with receptor of Escherichia coli (3t88), Staphylococcus aureus adhesion protein (4m01), Aspergillusflavus FAD glucose dehydrogenase (4ynt) and secreted aspartic protease from Candida albicans (1zap). One of the most favorable bindings of the ligand was its binding with 3t88 protein with estimated free energy of binding -4.07kcal/mol, and total intermolecular energy was of -5.27kcal/mol.

The ligand showed the inhibition constant (k_i) of 1.04mM. Figure 6 shows the binding of the ligand to the protein 3t88. A 2D plot was generated where ligand bond, non-ligand bond, and hydrogen bonds along with their length were mentioned (Figure 7). A HB plot [67,68] was generated to mention interactions with different amino acids of the protein (Figure 8).

In the studies by SwissDock, FullFitness and Gibbs free energy (ΔG) of each run (250 runs) of the docking were evaluated. Favorable binding modes were scored based on FullFitness and cluster formation. Ranking of the cluster was performed using the value of FullFitness. Table 7 exhibited the clustering results obtained from the docking of the ligand into 3t88 protein. The ligand showed FullFitness of -1339.98 kcal/mol and estimated ΔG of -6.85 kcal/mol for the most favorable interaction.

Based on the results of docking studies, it has been clearly expressed that the ligand and possibly its complexes showed favorable binding with 3t88, 4m01, 4ynt, 1zap. Hence, the ligand can be potential inhibitor to the pathogenic microorganisms like bacteria and fungi. This interaction could deactivate or kill the microorganisms. The characteristic feature of the ligand was represented in the presence of several active sites available for hydrogen bonding interaction. This theoretical analysis proposes the high biological activity of the organic ligand towards different bacteria or fungi.

The RAS oncogenes (HRAS, NRAS and KRAS) comprise the most frequently mutated class of oncogenes in human cancers (33%), stimulating intensive effort in developing anti-Ras inhibitors for cancer treatment. The protein-ligand interaction studies play a vital role in the structure based drug design in dry lab. Here, we show molecular modeling with docking results of the ligand as inhibitor of H-ras. The ligand showed favorable interaction binding with H-ras (121p) (Figure 9) with estimated free energy of binding -4.12kcal/mol, and total intermolecular energy was of -5.25 kcal/mol (Table 8). A 2D plot was generated where ligand bond, non-ligand bond, and hydrogen bonds along with their length were mentioned (Figure 10). A HB plot was generated to mention interactions with different amino acids of the protein (Figure 11).

FullFitness and Gibbs free energy (ΔG) of each run (250 runs) of the docking were estimated by Swissdock. Table 9 exhibited the clustering results obtained from the docking of the ligand into 121p protein. The ligand showed FullFitness of -1136.96kcal/mol and estimated ΔG of -6.32 kcal/mol for the most favorable interaction. Based on these analyses, the observed antitumor activity of the ligand and its complexes toward the proliferation rate of HepG2 cancer cells is proposed to be via H-ras inhibition.

3.2. Antibacterial activity

Biological activity of the investigated compounds (ligand and its metal complexes) was screened in-vitro against Gram positive bacteria (*S. aureus*) and Gram-negative bacteria (*E. coli*) by disc diffusion method [51]. The inhibition zone diameters are listed in Table 10 and represented graphically in Fig. 12. These compounds showed better antibacterial activity against Gram-negative bacteria. The results shown in Fig. 12 indicated that most complexes exhibited remarkable increase in activity than the parent ligand. Such increased activity of the metal complexes can be explained according to Tweedy's chelation theory [69]. Chelation reduce the polarity of the metal ion due to the partial sharing of its positive charge with the donor group and possible π -electron delocalization through the whole chelate ring system that is formed during complex formation. This process increases the lipophilic nature of the metal atom and hence increasing the hydrophobic nature and liposolubility of the complex favoring its permeation through the lipid layers of the microorganism, thus destroying them more aggressively. The antibacterial activity of the complexes can be ordered as $C3 > C1 > C2$ suggesting that the lipophilic behavior increases in the same order.

The complexes under investigation have: i) the same donating atoms which are N/O with the same coordination number. ii) the same chelate effect (all form two five membered chelating rings). iii) the same oxidation number in their complexes (M^{+2}). Therefore, the more effective factors are the nature of the central atom and the type of counter ions. The results, also, indicated that the complexes are more active against gram-negative than Gram- positive bacteria. The antibacterial results of the complex C3 was considered the most active compound. Therefore, the MIC screening of this complex was carried out. The MIC values were found to be 31 and 28 mg/ml against the microorganisms *C.albicans* and *E.coli*, respectively. These results indicated that C3 is more active against *E. coli* than *C.albicans*

3.3. Antifungal activity

The in-vitro antifungal activity of the ligand and its metal complexes was tested against *A. flavus* and *C. albicans*. The data of preliminary screening tests are listed in **Table 10** and shown in **Fig. 12**. The ligand (L) and its metal complex C2 had no effect against *A.* Complex C3 expressed a remarkable antifungal activity against *C. albicans* and *A. flavus*. The increased antifungal activity of some metal complexes may attributed to their high penetrating ability to the fungi cell wall [70].

3.4. Anticancer activity

The anticancer activity of the chalcone ligand (L) and its Pd(II) and Pt(II) complexes was determined in-vitro against the liver carcinoma cell line, HEPG2. The results of cytotoxic activity, compared with two standard drugs, are expressed as IC₅₀ which is the concentration required inhibiting a 50% of the cell growth when the cells are exposed to the compounds, **Table 11**. The concentration response profiles for the investigated compounds are given in **Fig. 13**. The cytotoxicity of the compounds against HEPG2 cell line is ordered in the sequence C1 > standard > C2>L>C3 compared with the standard drugs, doxorubicin. According to Shier [71] compounds with IC₅₀ within the range of 10-25 µg/ml are considered weak anticancer drugs, while those of IC₅₀ between 5 and 10 µg/ml are moderate and compounds of activity below 5.00 µg/ml are considered strong agents. Based on these facts, it is clear that the Pt(II) complex C1 and Pd(II) complex C2 exhibited excellent anticancer activity. The Pd(II) complex C3 exhibited a weak antitumor activity while the ligand exhibited medium activity according to Shier scale. The Structure-activity relationships for the tested compounds confirmed the following:

1- The activity of the Pd(II) complexes C2 and C3 can be ascribed to the difference in liability between the counter ion (chloride anions for C2 and acetate anions for C3) that alter the biochemical properties of these complexes [10] i.e the Pd(II) complexes were affected by the nature of the anion and the inhibitory activity was found to be increasing in the order:

Pd(II) complex C2 > Pd(II) complex C3; meaning that the chloride anions increased the anticancer activity compared with the acetate anions.

2- Pt(II) complex C1 with higher molar conductivity exhibited higher antitumor activity than Pd(II) complex C2. This indicated that the type of the metal ion may be the reason for this difference in activity [72]. The slightly higher toxicity of Pt(II) complex C1 ($IC_{50} = 3.08 \mu\text{g/ml}$) than the Pd(II) complex C2 ($IC_{50} = 3.98 \mu\text{g/ml}$) occurs because the ligand-exchange kinetics. The hydrolysis of leaving ligands in Pt(II) compounds is quite slow compared with that of Pd(II) compounds which give them a high kinetic stability and results in ligand-exchange reactions of minutes to day, rather than microseconds to seconds for many other coordination compounds [73].

3- The obtained results indicated also that the metal complexes C1 and C2 are more effective than the chalcone ligand towards the tested cell line. This indicated that the complexation to the metal ion enhanced the anticancer behaviour. This may be attributed to the increase in conjugation in the ligand moiety on complexation [74]. On the other hand, the Pd(II) complex C3 exhibited less activity than the ligand while the reason of such decreased activity is ambiguous indicating that relationship between structure and activity is extremely complex.

3.5. Antioxidant

Pd(II), Pt(II) as well as the free ligand were tested for their antioxidant activities. The radical scavenging ability of these compounds was evaluated against the DPPH stable free radical, **Fig. 14**. The DPPH assay of these compounds shown in **Table 11** indicated that complexes C1-C3 exhibited higher antioxidant activity compared to the standard, ascorbic acid. The IC_{50} values of complexes C1-C3 indicated that the compounds showed antioxidant activity in the order C1>C3>C2 i.e complex C1 showed a higher antioxidant activity compared to complexes C2 and C3. Also, the

scavenging effect of the metal complexes is lower compared to the free ligand.

4. Conclusion

We have reported the synthesis of Pt(II) and Pd(II) chalcone complexes. The structural characterization of the synthesized compounds was made by using the elemental analyses, spectroscopic methods, conductance studies and thermal analysis. The chalcone ligand behaved as a neutral bidentate ligand through oxygen and nitrogen atoms of carbonyl and azomethine groups, respectively. Square planar geometry for the complexes was reported. All complexes are electrolytes. The biological activity screening showed that the complexes have increased activity compared with the ligand against the tested bacteria and fungi. The cytotoxicity of the ligand and its complexes against HEPG2 cancer cell line has been studied. Pt(II) complex C1 exhibited excellent anticancer activity which is more active even than the standard drug (doxorubicin). A structure-reactivity relationship was proposed to evaluate the activity of prepared compounds. The radical scavenging ability of the studied compounds was tested against the DPPH stable free radical. The DPPH assay indicated that complexes C1-C3 exhibited higher antioxidant activity compared to the standard (ascorbic acid). IC₅₀ values showed antioxidant activity in the order C1>C2>C3 i.e complex C1 showed a higher antioxidant activity compared to complexes C2 and C3. The metal complexes have less scavenging effect compared to the free ligand.

Molecular Docking studies were performed in DockingServer and SwissDock. X-ray crystallographic structures of the proteins were retrieved from Protein Data Bank (PDB), and used as drug target protein. Molecular visualization was performed using UCSF Chimera. The ligand showed favorable binding with the bacterial receptor protein 3t88 and the oncogene protein H-ras. Conclusively our results strongly suggest that the ligand is a potent anti H-ras agent as ascertained by its potential

interaction with H-ras. This scientific hypothesis might provide a better insight to control carcinogenesis as well as to control solid cancer growth and metastasis.

Acknowledgement

The authors would like to thank Tanta University (Grant No: Tu 03-13-01) for the financial support of this project. We would like to extend our grateful thanks to Prof. Dr Tarek Mostafa for his assistance in evaluating the antioxidant activities.

References

- [1] A.S. Abu-Surrah, H.H. Al-Sa'doni, M.Y. Abdalla, *Cancer Ther.* 6 (2008) 1
- [2] E.J. Gao, C. Liu, M.C. Zhu, H.K. Lin, Q. Wu, L. Liu, *Anti Cancer Agents Med. Chem.* 9 (2009) 356
- [3] P.I. da, S. Maia, A.G. de, A. Fernandes, J.N. Silva, A.D. Andricopulo, S.S. Lemos, E.S. Lang, U. Abram, V.M. Deflon, *J. Inorg. Biochem.* 104 (2010) 1276
- [4] J. Schulz, A.K. Renfrew, I. Cisarova, P.J. Dyson, P. Stepnicka, *Appl. Organomet. Chem.* 24 (2010) 392
- [5] E. Gao, M. zhu, Y. Huang, L. Liu, H. Liu, F. Liu, S. Ma, C. Shi, *Eur. J. Med. Chem.*, 45 (2010) 1034
- [6] F.Rocha, C. Barra, A.Netto, A. Mauro, I. Carlos, R. Frema, S. Ananias, M. Quilles, A. Stevanato, M. da Rocha, *Eur. J. Med. Chem.*, 45 (2010) 1698
- [7] M. Juribasic, K. Molcanov, B. Kojic-Prodic, L. Bellotto, M. Kralj, F. Zani,

- L. Tusek-Bozic, *J. Inorg. Biochem.*, 105 (2011) 867
- [8] A.I. Matesanz, J. Perles, P. Souz, *Dalton Trans.* 41 (2012) 12538
- [9] K. Karami, M. Hosseini kharat, H. Sadeghi-Aliabadi, J. Lipkowski, M. Mirian,
Polyhedron, 50 (2012) 187
- [10] H. El-Boraey, *Spectrochim. Acta A*, 97 (2012) 255
- [11] N. T. Abdel Ghani, A. M. Mansour, *Eur. J. Med. Chem.*, 47 (2012) 399; A. Mansour, M. Mohamed, *Inorg. Chimica Acta*, 423 (2014) 373; A. Mansour, N. Abdel-Ghani, *Inorg. Chimica Acta*, 438 (2015) 76
- [12] N. Cutillas, G.S. Yellol, C. de Haro, C. Vicente, V. Rodriguez, J. Ruiz, *Coord. Chem. Rev.* 257 (2013) 2784
- [13] A. El-Husseiny, H. Hassan, *Spectrochim. Acta, A*, 103 (2013) 232
- [14] N. Ozbek, S. Alyar, H. alyar, E. Sahin, N. Karacan, *Spectrochim. Acta A*, 108 (2013) 123
- [15] M. Jagadeesh, H. Rashmi, Y. Rao, A. S. Reddy, B. Prathima, P. Devi, A. V. Reddy, *Spectrochim. Acta A*, 115 (2013) 583
- [16] J. Zhang, L. wang, S.Y. Liu, F. Zhang, J. Du, L. Li, S. Wang, S. Li, G. Zhou, *Russ. J. Coord. Chem.*, 40 (2014) 115
- [17] D.L. Stojković, V.V. Jevtić, G.P. Radić, D.V. Todorović, M. Petrović, M. Zarić, I. Nikolić, D. Baskić, S.R. Trifunović, *J. Inorg. Biochem.* 143 (2015) 111

- [18] M. Gaber H. El-Ghamry S. K. Fathalla, *Spectrochim. Acta A*, 139 (2015) 396
- [19] D. Gutierrez, S. Bernes, G. Hernandez, O. Portillo, G. Moreno, M. Sharma,
P. Sharma, R. Gutierrez, *J. Coord. Chem.*, 68 (2015) 3805
- [20] D. Ajloo, M. Moghadam, K. Ghadimi, M. Ghadamgahi, A. Saboury, A. Divsalar, M. Sheikh-Mohammadi, K. Yousefi, *Inorg. Chimica Acta*, 430 (2015) 144
- [21] H. Pruchnik, T. Lis , M. Latocha, A. Zielińska, F. P. Pruchnik, J. *Inorg. Biochem.*, 156 (2016) 14
- [22] M. Zhu, X. Cui, S. Zhang, L. Liu, Z. Han , E. Gao, *J. Inorg. Biochem.* 157 (2016) 34
- [23] B. Mavroidi, M. Sagnou , M. Paravatou-Petsotas , M. Pelecanou, *Inorg. Chimica Acta*, 444 (2016) 63
- [24] M. Amir, S. Khan , F. Hayat , A. Hassan, I. Butler , Z. Rehman, *Inorg. Chimica Acta*, 451(2016) 31
- [25] C. Barra, F. Rocha, L. Morel, A. Gautier, S. Garrido, A. Mauro, R. Frem,
A. Netto, *Inorg. Chimica Acta*, 446 (2016) 54
- [26] A. Al-Dawood, N. El-Metwaly, H. El-Ghamry, *J. Mol. Liq.*, 220 (2016) 311
- [27] L. Via, G. Gia, G. Chiarello, M. Ferlin, *Eur. J. Med. Chem.*, 44 (2009) 2854
- [28] Z. Ratkovic, Z. Juranic, T. Stanojkovic, D. Manojlovic, R. Vukicevic, N. Radulovic, M. Joksovic, *Bioorg. Chem.*, 38 (2010) 26

- [29] L. Tavares, S. Johann, T. Alves, J. Guerra, *Eur. J. Med. Chem.*, 46 (2011) 4448
- [30] M. Abdel-Aziz, S. Park, G. Abuo-Rahma, M. A. Sayed, Y. Kwon, *Eur. J. Med. Chem.* 69 (2013) 427
- [31] P. Singh, A. Anand, V. Kumar, *Eur. J. Med. Chem.* 85 (2014) 758
- [32] D. Mahapatra, S. Bharti, V. Asati, *Eur. J. Med. Chem.* 98 (2015) 69
- [33] M. Kaveri, R. Prabhakaran, R. Karvembu, K. Natarajan, *Spectrochim. Acta A*, 61 (2005) 2915
- [34] M. Gaber, S.A. El-Daly, Y.S. El-Sayed *J. Mol. Struct.*, 922 (2009) 51
- [35] M. Muthukumar, P. Viswanathamurthi, *J. Coord. Chem.*, 63 (2010) 1263
- [36] P. Rishikesh, S. Dubey, R. Gaur, R. Koiri, B. Maurya, S. Trigun, L. Mishra, *Polyhedron*, 29 (2010) 1055
- [37] M. Kalanithi, M. Rajarajan, P. Tharmaraj, C. Sheela, *Spectrochim. Acta A*, 87 (2012) 155
- [38] J. Da Silva, A. Recio Despaigne, S. Louro, C. Bandeira, E. Souza-Fagundes, H. Beraldo, *Eur. J. Med. Chem.*, 65 (2013) 415
- [39] M. El Sayed Aly, H. Fodah, S. Saleh, *Eur. J. Med. Chem.*, 76 (2014) 517
- [40] M. Gaber, S.Al-Daly, T. Fayed, Y. El-Sayed, *J. Lumin.*, 157 (2015) 1

- [41] Y.S. El-Sayed, M. Gaber, Spectrochim. Acta A, 137 (2015) 423
- [42] A. K. Singh, G. Saxena, S. Dixit, Hamidullah, S. K. Singh, S. K. Singh,
M. Arshad, R. Konwar, J. Mol. Struct., 1111 (2016) 90
- [43] R. Křikavová, J. Vančo, Z. Trávníček, J. Hutýra, Z. Dvořák, J. Inorg. Biochem. 163 (2016) 8
- [44] Bikadi, Z., Hazai, E. Application of the PM6 semi-empirical method to modeling proteins enhances docking accuracy of AutoDock J. Cheminf. **1**, 15 (2009)
- [45] G. M. Morris, D. S. Goodsell, et al. *Automated docking using a Lamarckian genetic algorithm and an empirical binding free energy function* Journal of Computational Chemistry **19 (14)**, 1639-1662 (1998)
- [46] F. J. Solis and R. J. B. Wets *Minimization by Random Search Techniques* Mathematics of Operations Research **6 (1)**, 19-30 (1981).
- [47] Grosdidier A, Zoete V, Michielin O (2011a) SwissDock, a protein-small molecule docking web service based on EADockDSS. Nucleic Acids Res 39:W270–W277.
- [48] Grosdidier A, Zoete V, Michielin O (2011b) Fast docking using the CHARMM force field with EADock DSS. J ComputChem32:2149–2159.
- [49] Grosdidier A, Zoete V, Michielin O (2007) EADock: docking of small molecules into protein active sites with a multiobjective evolutionary optimization. Proteins 67:1010–1025.
- [50] Pettersen EF, Goddard TD, Huang CC, Couch GS, Greenblatt DM, Meng EC, Ferrin TE (2004) UCSF chimera—a visualization system for exploratory research and analysis. J ComputChem 25:1605–1612.
- [51] T. Pridham, L. Lindenfelser, O. Shotwell, F. Stodola, R. Benedict, C. Foley, P. Jacks, W. Zaumeyer, W. Perston, J. Mitchell, Phytopathology, 46 (1956) 568

- [52] S. Shadomy, I. Epsinel, R. Cartwright, Laboratory studies agents: Susceptibility test and bioassays. A. Lennette, W. Balows, H. Hausler, S. Shadomy, 4th ed., Manual of Clinical Microbiology, Little Brown Co., Boston.1985
- [53] P. Skehan, R. Storeng, J. Natl, Cancer Inst. 82 (1990) 1107
- [54] National committee for Clinical laboratory standards, NCCLS approval Standard document M2-A7, Vilanova, PA, 2000.
- [55] HyperChem, Release 8.03 for Windows, Molecular modeling system, Hypercube
- [56] W.J. Geary, Coord. Chem. Chem., 7 (1971) 81
- [57] A. B. P. Lever, *Inorganic Electronic Spectroscopy*, second ed. Elsevier, Amsterdam, 1982, p 544-552.
- [58] O. A. Ali, Spectrochim. Acta A, 121 (2014) 188
- [59] A.W. Coats, J. P. Redfern, Nature, 201 (1964) 68
- [60] M. Gaber, Y. El-Sayed , K. El-Baradie, R. Fahmy, Spectrochim. Acta, A, 107, (2013) 359; M. Gaber , Y. S. El-Sayed , K. El-Baradie, R. Fahmy, J. Mol. Struct., 1032 (2013) 185
- [61] M. Gaber , H. El-Ghamry, F. Atlam, S. Fathalla, Spectrochim. Acta A, 137, (2015) 919
- [62] N Abdel Ghani, A. Mansour, Spectrochim. Acta A, 81 (2011) 529
- [63] R. Pearson, Journal of Organic Chemistry, 54 (1989) 1423
- [64] S. Sagdinc, B. Koksoy, F. Kandeirli, S. Bayari, J. Mol. Struct, 917 (2009) 63
- [65] J. Padmanabhan, R. Parthasarathi, V. Subramanian, J. Phys. Chem., A, 111 (2007) 1358

- [66] T. A. Yousef, O.K. Alduaij, S.A.Ahmed, G.M. Abu El-Reash, O.a. El-Gammal, *J. Mol. Struct.*, 1119 (2016) 351
- [69] B.G. Tweedy, *Phyto. Pathol.*, 55 (1964) 910
- [70] R. John, A. Sreekanth, V. Rajakannan, T.A. Ajith, M.R. Kroup, *Polyhedron*, 23, (2004) 2549
- [71] W.T. Shier, *Mammalian Cell Culture on \$5 a Day: A Lab Manual of Low Cost Methods*, University of the Philippines, Los Banos, 1991.
- [72] X. Riera, V. Moreno, C. Ciudad, V. Noe, M. Font-Bardia, X. Solans, *Bioinorg. Chem. Appl.*, 2007 (2007) 1
- [73] J. Reedijk, *Inorg. Chim. Acta*, 198 (1992) 873
- [74] K. Dhahagani, S. Kumar, G. chakkaravarthi, K. Anitha, J. Rajesh, A. Ramu, G. Rajagopal, *Spectrochim. Acta A*, 117 (2014) 87

Table 1: IR spectral bands of the chalcone ligand and its metal complexes

Comp.	$\nu(\text{H}_2\text{O})$	$\nu(\text{C}=\text{O})$	$\nu(\text{C}=\text{N})$	$\nu(\text{M}-\text{O})$	$\nu(\text{M}-\text{N})$
L1	-	1650	1611	-	-
C1	3449	1630	1601	630	555
C2	3450	1608	1600	662	558
C3	3445	1629	1600	597	560

Table 2: Thermal analyses (DTA & TGA) of the metal complexes.

No.	FW (M wt)	TG range (°C)	DTG max(°C)	(Calc.) found mass loss %	Assignment
C1	[(L1) ₂ Pt]Cl ₂ .2H ₂ O C ₃₂ H ₃₅ Cl ₂ N ₄ O _{3.5} Pt (806.6)	30-93	62	(4.46) 3.98	- Loss of lattice water
		93-316	314	(14.30) 13.93	- Loss of lattice chloride + one N(CH ₃) ₂ moiety
		316-428	389	(43.62) 43.11	-Further decomposition of ligand leaving PtO+8C as residue.
C2	[(L1) ₂ Pd]Cl ₂ .0.5H ₂ O C ₃₂ H ₃₃ Cl ₂ N ₄ O _{2.5} Pd 690.96	30-85	50	(1.30) 1.48	- Loss of one lattice water
		163-252	228	(14.47) 14.85	- Loss of lattice chloride + 2CH ₃
		252-447	312	(54.49) 55.74	-Further decomposition of ligand leaving PdO +7C as residue.
C3	[(L1) ₂ Pt](CH ₃ COO) ₂ . CH ₃ OH C ₃₇ H ₄₂ N ₄ O ₇ Pd 761.17	25-76	42	(4.20) 3.84	- Loss of lattice MeOH
		76-283	266	(31.34) 31.72	-Loss of two acetato+ one N(CH ₃) ₂ +C ₆ H ₅
		283-423	396	(37.42) 36.66	-Further decomposition of ligand leaving PdO +7C as residue.

Table 3: Thermodynamic data of the thermal decomposition of chalcone complexes (C1-C3) at heating rate 10 °C/ min.

<i>No.</i>	<i>n</i>	<i>r</i>	<i>E</i>	<i>A(s-1)</i>	<i>ΔG</i>	<i>-ΔS</i>	<i>ΔH</i>
C1	1	0.9650	168.1	0.006	264.1	0.296	165.3
C2	1	0.9956	123.4	12.63	198.3	0.233	120.6
C3	1	0.9989	85.4	5003.6	143.7	0.183	82.6

kJ mol⁻¹ for *E*, *ΔG* and *ΔH*; Jmol⁻¹ K⁻¹ for *ΔS*

Table 4. The calculated quantum chemical parameters for the ligand and its Pd(II) complex

Compd	E_{HOMO} eV	E_{LUMO} eV	ΔE eV	χ eV	η eV	σ eV⁻¹	Pi eV	ω	ΔN_{max}
L	-9.000	-3.334	5.666	6.167	2.833	0.353	- 6.167	6.71	2.177
Pd complex	-7.291	-1.105	6.186	4.189	3.093	0.323	- 4.189	2.84	1.354

$\Delta E = E_{LUMO} - E_{HOMO}$, $\eta = \Delta E/2$; $\sigma = 1/\eta$; $Pi = -(E_{HOMO} + E_{LUMO})/2$; $\chi = -Pi$; ω

Table 5. Some energetic properties of the ligand and it complex.

The assignment of the theoretical parameters	L	Pd complex
Total energy Kcal/mol	-62634.4	-151264.40
Binding energy Kcal/mol	-3684.294	-7748.354
Electronic Energy Kcal/mol	-434645.63	-1499067.46
Heat of Formation Kcal/mol	169.136	48.5079
Dipole moment (Debye)	3.421	5.788
HOMO (ev)	-9.000	-7.291
LUMO (ev)	-3.334	-1.105

Table 6

Energy values obtained for the molecular docking of the ligand with receptor of Escherichia coli (3t88), Staphylococcus aureus adhesion protein (4m01), Aspergillusflavus FAD glucose dehydrogenase (4ynt) and secreted aspartic protease from Candidaalbicans (1zap).

Protein PDB	Est. free energy of binding (kCal/mol)	Est. inhibition constant (Ki) (mM)	vdW + Hbond + desolv energy (kCal/mol)	Electrostatic energy (kCal/mol)	Total intemolec. energy (kCal/mol)	Frequency	Interact. surface
3t88	-4.07	1.04	-5.14	-0.13	-5.27	70%	689.219
4m01	-2.75	9.71	-3.68	-0.20	-3.88	30%	614.193
4ynt	-6.91	8.56 x10 ⁻³	-8.07	-0.01	-8.08	10%	720.623
1zap	-5.20	155.30 x10 ⁻³	-6.25	-0.07	-6.31	40%	715.623

Table 7. Clustering results obtained from the docking of the ligand into receptor of Escherichia coli (3t88) by SwissDock.

Receptor	No. of SwissDock clusters	Cluster rank	FullFitness (kcal/mol)	Estimated ΔG (kcal/mol)
3t88	40 (250 runs)	1	-1339.98	-6.85
		2	-1337.67	-6.65
		3	-1336.14	-6.69
		4	-1333.63	-6.65
		5	-1333.63	-6.65

Table 8
Energy values obtained for the molecular docking of the ligand against H-ras (PDB: 121P) in cancer.

Protein PDB	Est. free energy of binding (kCal/mol)	Est. inhibition constant (Ki) (mM)	vdW + Hbond + desolv energy (kCal/mol)	Electrostatic energy (kCal/mol)	Total intemolec. energy (kCal/mol)	Frequency	Interact. surface
H-ras	-4.12	952.52 $\times 10^{-3}$	-4.89	-0.36	-5.25	40%	677.049

Table 9 Clustering results obtained from the docking of the ligand into H-ras (121p) by SwissDock.

Protein	No. of SwissDock clusters	Cluster rank	FullFitness (kcal/mol)	Estimated ΔG (kcal/mol)
H-ras (121p)	45 (250 runs)	1	-1136.96	-6.32
		2	-1136.96	-6.32
		3	-1135.81	-6.28
		4	-1133.90	-6.17
		5	-1133.90	-6.17

Table 10. Antibacterial and antifungal results of the ligand (L) and its metal complexes.

Comp.	inhibition Zone diameter (mm)			
	a	b	C	d
L1	11	0	13	11
C1	12	9	13	12
C2	11	0	12	11
C3	15	9	14	13

(a) *C.albicans*, (b) *A.flavus*, (c) *E.coli* and (d) *S.aureus*.

Table 11. IC₅₀ values calculated from the *In vitro* antitumor activities against HEPG2 cell line and antioxidant results against DPPH

Compound	IC ₅₀ (μg/mL)	IC ₅₀ (mg/ml)
	HEPG2	DPPH
L1	6.53	43.92
C1	3.08	48.92
C2	13	63.54
C3	3.98	20.02
Dox ₁	3.1	-

¹ doxorubicin; standard cytotoxin drug

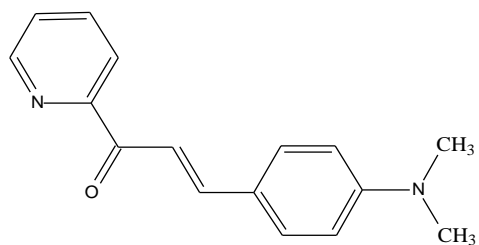


Fig. 1 The structure of the ligand.

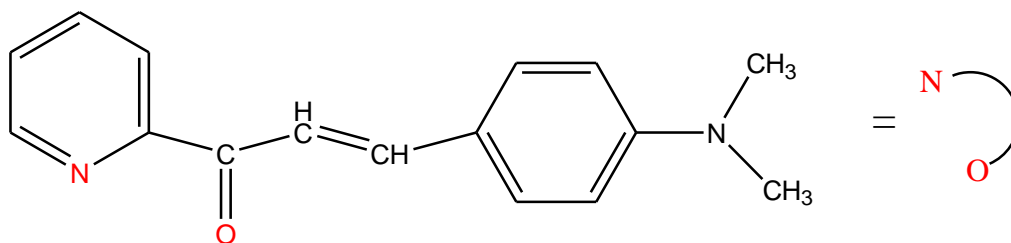
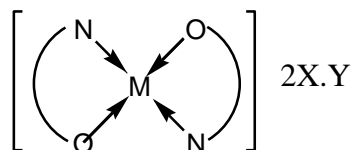


Fig. 1. The structure of the chalcone compound (L).



- C1, M = Pt, X = Cl, Y = 2H₂O
 C2, M = Pd, X = Cl, Y = 0.5H₂O
 C3, M = Pd, X = AcO, Y = MeOH

Fig. 2. The structures of the complexes.

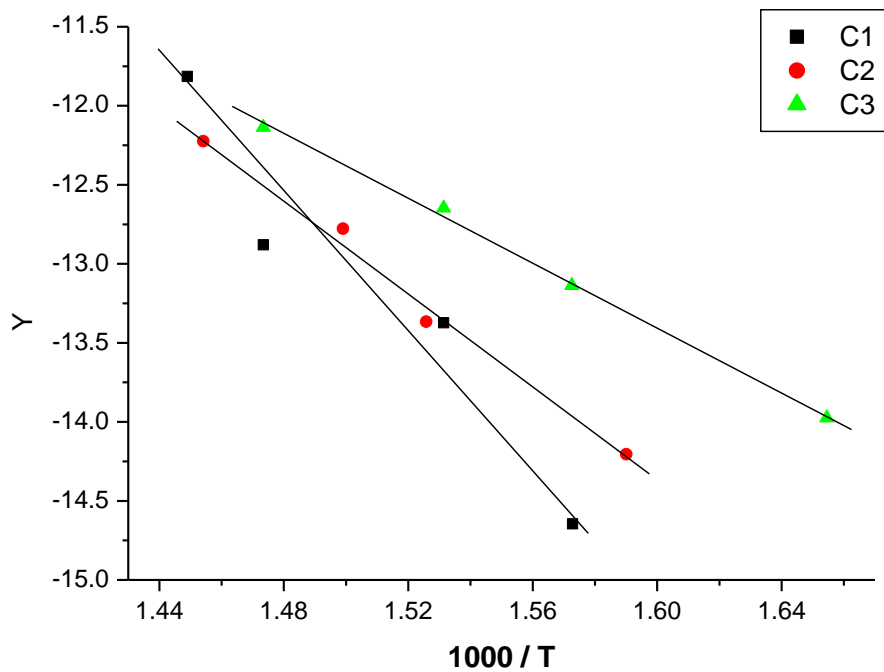
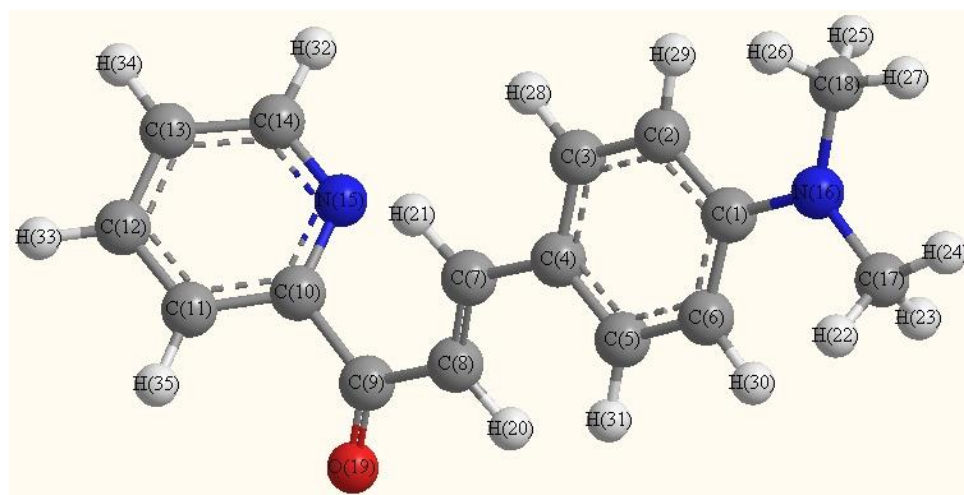


Fig. 3. Coats-Redfern plot for complexes C1-C3. where, $Y = [1 - (1 - \alpha)^{1-n}] / (1-n) T^2$ for $n \neq 1$ or $Y = [-\ln(1 - \alpha)] / T^2$ for $n = 1$

A



B

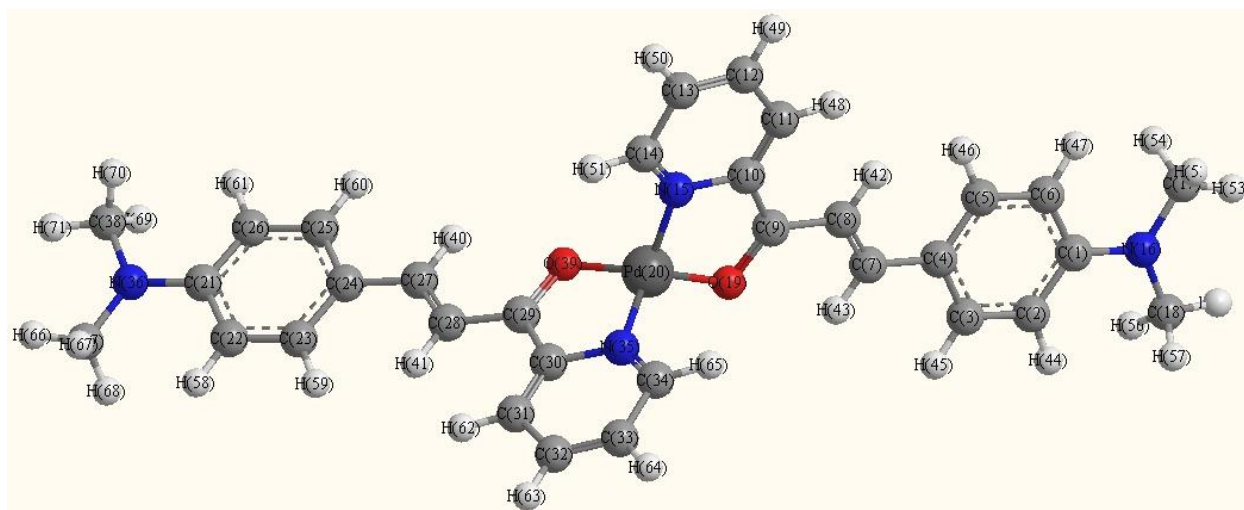
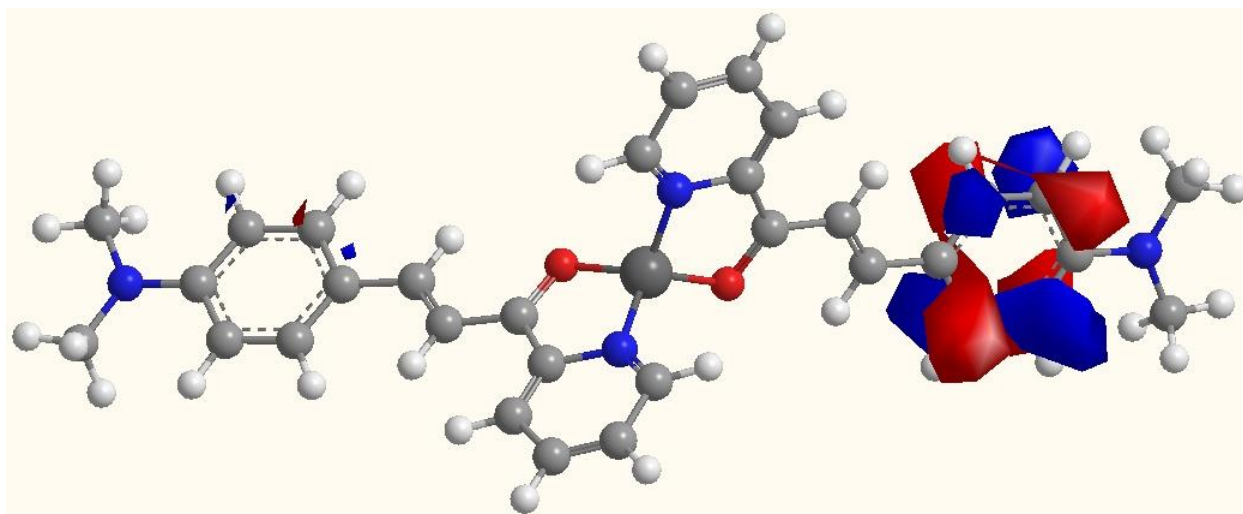
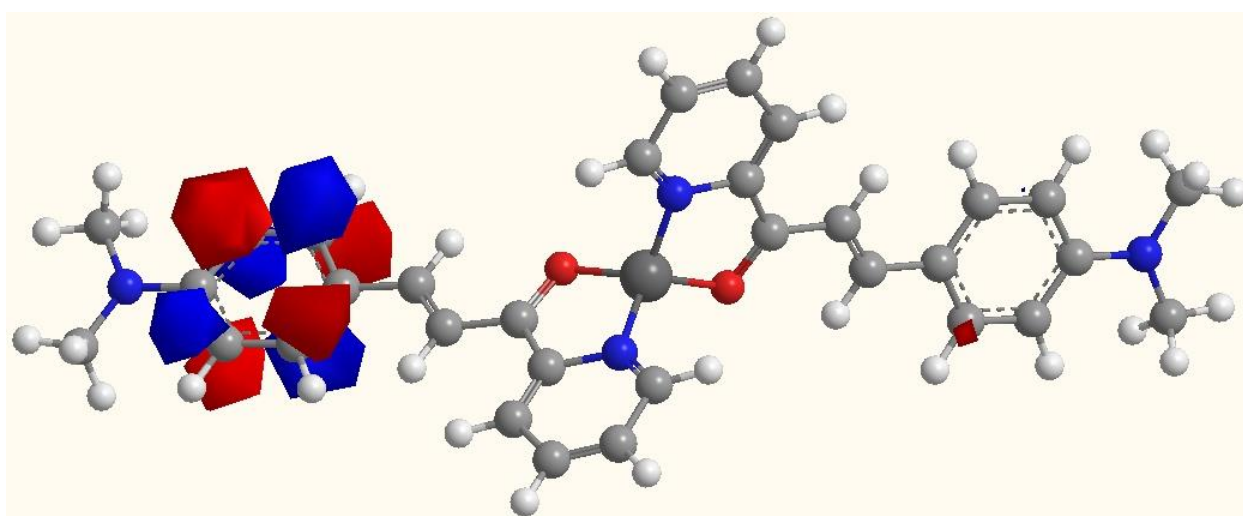


Fig. 4 The modeling structures of the ligand (A) and its Pd(II) complex B.



HOMO of Pd Complex



LUMO of Pd complex

Fig. 5. The HOMO-LUMO of the ligand and its Pd(II) complex.

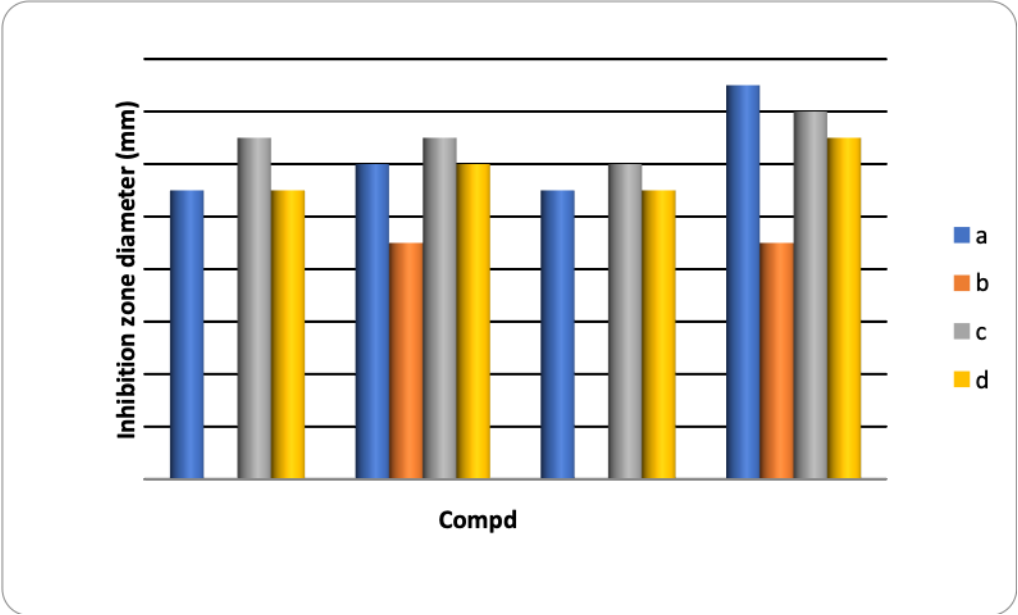


Fig. 12. Effect of ligand and its metal complexes toward (a) *C.albicans*, (b) *A.flavus*,
(c) *E.coli* and (d) *S.aureus*.

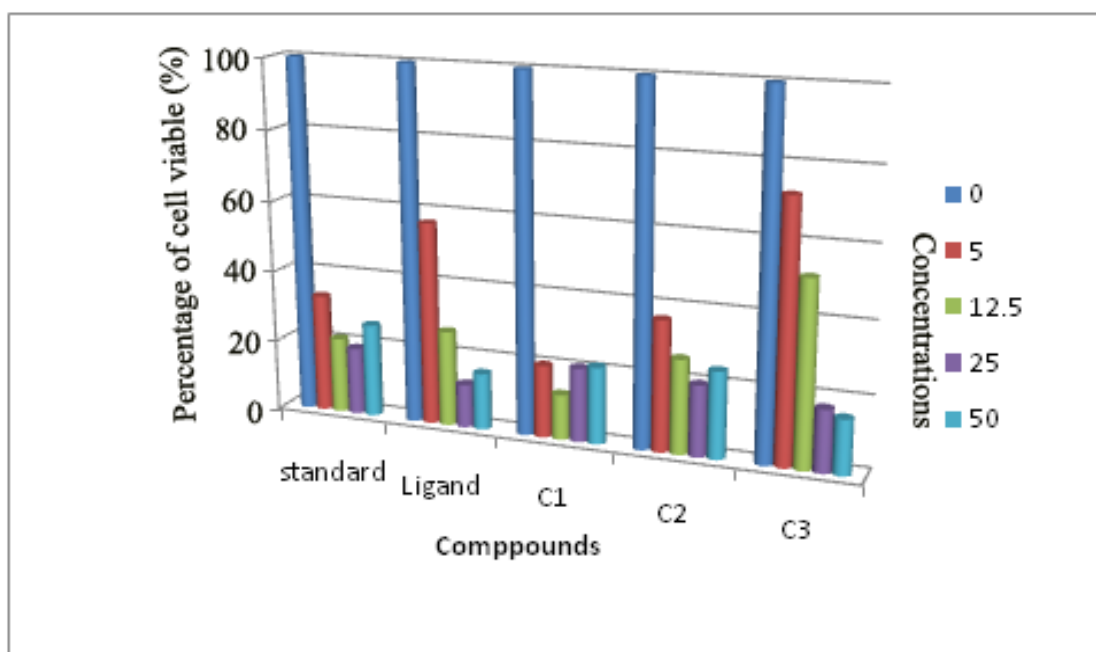


Fig. 13. Effect of chalcones ligand and its Pt(II) and Pd(II) complexes as surviving fraction of HEPG2 tumor cell.

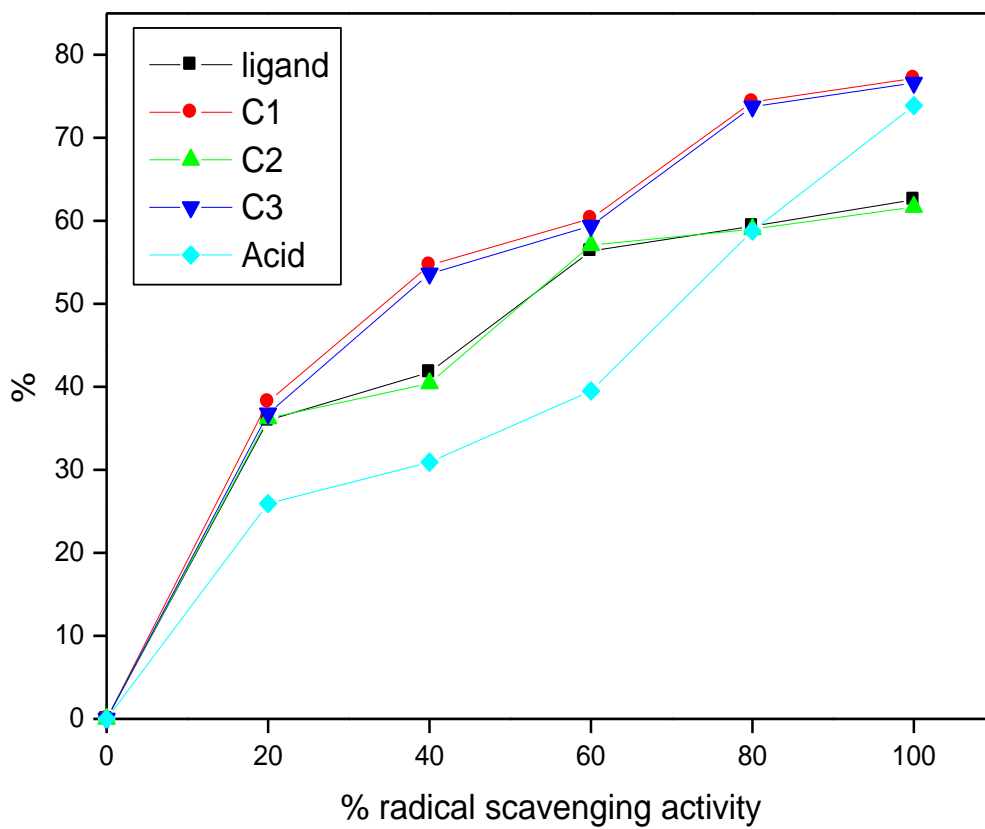


Fig.14. The scavenging activity of the ligand and its complexes.